

Experimental Study of the NaK $3^1\Pi$ State

E. Laub,¹ I. Mazsa,² S. C. Webb,³ J. La Civita, I. Prodan, Z. J. Jabbour,⁴ R. K. Namiotka,⁵ and J. Huennekens

Dept. of Physics, 16 Memorial Dr. East, Lehigh University, Bethlehem, Pennsylvania 18015

Received August 3, 1998

We report the results of an optical–optical double resonance experiment to determine the NaK $3^1\Pi$ state potential energy curve. In the first step, a narrow band cw dye laser (PUMP) is tuned to line center of a particular $2(A)^1\Sigma^+(\nu', J') \leftarrow 1(X)^1\Sigma^+(\nu'', J'')$ transition, and its frequency is then fixed. A second narrowband tunable cw Ti:Sapphire laser (PROBE) is then scanned, while $3^1\Pi \rightarrow 1(X)^1\Sigma^+$ violet fluorescence is monitored. The Doppler-free signals accurately map the $3^1\Pi(\nu, J)$ ro-vibrational energy levels. These energy levels are then fit to a Dunham expansion to provide a set of molecular constants. The Dunham constants, in turn, are used to construct an RKR potential curve. Resolved $3^1\Pi(\nu, J) \rightarrow 1(X)^1\Sigma^+(\nu'', J'')$ fluorescence scans are also recorded with both PUMP and PROBE laser frequencies fixed. Comparison between observed and calculated Franck–Condon factors is used to determine the absolute vibrational numbering of the $3^1\Pi$ state levels and to determine the variation of the $3^1\Pi \rightarrow 1(X)^1\Sigma^+$ transition-dipole moment with internuclear separation. The recent theoretical calculation of the NaK $3^1\Pi$ state potential reported by Magnier and Millié (1996, *Phys. Rev. A* **54**, 204) is in excellent agreement with the present experimental RKR curve. © 1999 Academic Press

I. INTRODUCTION

One photon absorption spectra involving transitions between two electronic states of alkali diatomic molecules are extremely complicated due to small vibration and rotation constants and the fact that many ground state ro-vibrational levels are thermally populated at the temperatures necessary to produce a sufficient vapor pressure. The complexity of the spectra is greatly reduced by the use of the optical–optical double resonance (OODR) technique. In OODR, the first laser (PUMP) is used to populate one ro-vibrational level of an intermediate electronic state. The second laser (PROBE) is then used to excite these molecules to a higher electronic state. Absorption of the PROBE photon can be monitored by detecting direct fluorescence from the upper level (1–4), fluorescence from nearby levels of the same or another electronic state populated by collisions (5–9), fluorescence from atomic levels populated by predissociation or collisional energy transfer (4), ions produced by photoionization or various collisional mechanisms involving the upper level (2, 9–13),

or rotations of the PROBE laser polarization (14–15). Because only one ro-vibrational level is used as a starting point for this PROBE step, the spectra consist of very simple patterns which allow easy identification of the electronic states involved, as well as the determination of molecular constants. In the case of homonuclear molecules, the OODR technique allows access to states of the same gerade/ungerade (*g/u*) parity as the ground state. In a variation of this technique, called perturbation-facilitated optical–optical double resonance (PFOODR), mutually perturbed (mixed) singlet–triplet intermediate levels allow access to higher spin–triplet states (16).

In a recent work (4), we have used the OODR technique to study the $6^1\Sigma^+$ state of the heteronuclear alkali molecule NaK. In this experiment, the PUMP laser was used to excite specific $2(A)^1\Sigma^+(\nu', J') \leftarrow 1(X)^1\Sigma^+(\nu'', J'')$ transitions. The intermediate state $2(A)^1\Sigma^+(\nu', J')$ levels were then excited further using the PROBE laser tuned to various $6^1\Sigma^+(\nu, J' \pm 1) \leftarrow 2(A)^1\Sigma^+(\nu', J')$ transitions. Due to the selection rules $\Delta J = \pm 1$ for $\Sigma \leftrightarrow \Sigma$ transitions ($\Sigma^+ \leftrightarrow \Sigma^+$ but $\Sigma^+ \leftrightarrow \Sigma^-$) and $\Delta J = 0, \pm 1$ for $\Pi \leftrightarrow \Sigma$ transitions, the pattern of double lines allowed the easy identification of the upper state as a Σ^+ state. During the course of these measurements, a few sets of triple lines were also observed. Since the presence of strong Q ($\Delta J = 0$) lines, in addition to R and P ($\Delta J = \pm 1$) lines, implies that $\Delta\Lambda = 1$, it is clear that these triple lines are associated with transitions to a $^1\Pi$ state (17). We have now carried out detailed studies of this $^1\Pi$ state (which has now been identified as the $3^1\Pi$ state,

¹ Present address: Wavefront Research Inc., 616 W. Broad St., Bethlehem, PA 18018-5221.

² Present address: Teradyne, 321 Harrison Ave., Boston, MA 02118.

³ Present address: Dept. of Physics, Randall Laboratory, University of Michigan, Ann Arbor, MI 48109.

⁴ Present address: Automated Production Technology Division, Sound A147, NIST, Gaithersburg, MD 20899.

⁵ Present address: Dept. of Physics, Drew University, Madison, NJ 07940.

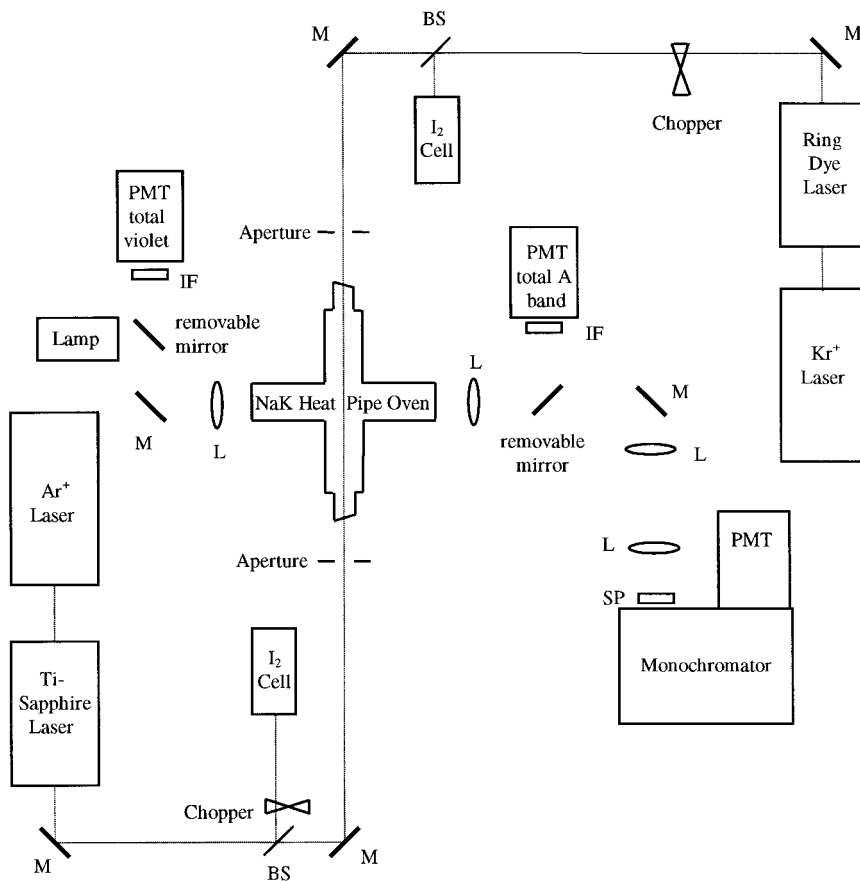


FIG. 1. Experimental setup. L, M, and BS represent lens, mirror, and beam splitter, respectively, while SP, IF, and PMT refer to short-pass filter, interference filter, and photomultiplier tube, respectively.

dissociating to the $\text{Na}(3S_{1/2}) + \text{K}(3D_{3/2})$ separated atom limit), and these results are reported in the present manuscript.

This manuscript is organized as follows. Section II describes the experimental setup and procedure. Our analysis and results for the $3^1\Pi$ state molecular constants, RKR curve, and the $3^1\Pi(v, J, f) \rightarrow 1(X)^1\Sigma^+(v', J, e)$ transition Franck–Condon factors are presented in Section III. Section IV compares the present experimental results with recent theoretical calculations.

II. EXPERIMENTAL

The experimental setup is shown in Fig. 1. The sodium–potassium mixture is contained in a crossed heat-pipe oven (at a temperature in the range 357–402°C) using argon as a buffer gas ($P = 0.4$ –1.2 Torr). A single-mode ring dye laser (Coherent model 699-29), using LD700 dye and pumped by

a 5 W krypton ion laser, is used as the PUMP laser to excite specific $2(A)^1\Sigma^+(v', J') \leftarrow 1(X)^1\Sigma^+(v'', J'')$ transitions. A single mode Ti:Sapphire laser (Coherent model 899-29), pumped by a 10 W argon ion laser, is used as the PROBE laser on the $3^1\Pi(v, J', f) \leftarrow 2(A)^1\Sigma^+(v', J', e)$ and $3^1\Pi(v, J' \pm 1, e) \leftarrow 2(A)^1\Sigma^+(v', J', e)$ transitions. The two laser beams counterpropagate through the heat-pipe oven, producing Doppler-free lines of approximately 60–180 MHz linewidth. The PUMP laser frequency is set to line center of a particular $2(A)^1\Sigma^+(v', J') \leftarrow 1(X)^1\Sigma^+(v'', J'')$ transition by monitoring total $A \rightarrow X$ band fluorescence, emitted at right angles to the laser propagation axis, with a free-standing photomultiplier tube (Hamamatsu R406, 400–1100 nm S-1 response) equipped with a 700–1000 nm interference filter (“PMT – total A band” in Fig. 1). The PROBE laser is then scanned and absorption of PROBE laser photons is monitored by detecting $3^1\Pi(v, J, f) \rightarrow 1(X)^1\Sigma^+(v', J, e)$ or $3^1\Pi(v, J, e) \rightarrow 1(X)^1\Sigma^+(v', J \pm 1, e)$ violet fluorescence emerging from the opposite side arm of the heat-pipe oven. This latter

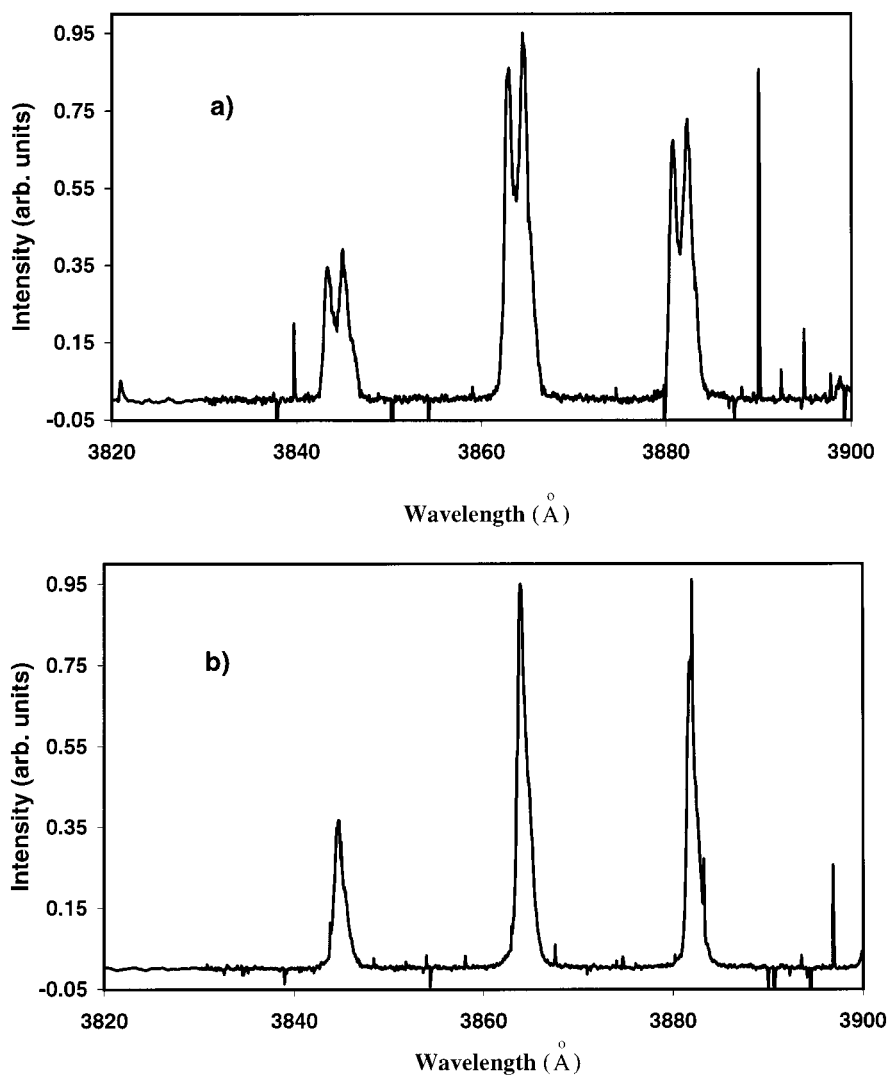
NaK $3^1\Pi \rightarrow 1(X)^1\Sigma^+$ Resolved Fluorescence

FIG. 2. Resolved fluorescence scans. (a) First few lines of the NaK $3^1\Pi$ ($v = 12, J = 29, e$) $\rightarrow 1(X)^1\Sigma^+$ ($v', J \pm 1, e$) fluorescence series. The selection rule $\Delta J = \pm 1$ for $^1\Pi$ (e parity) $\rightarrow ^1\Sigma^+$ (e parity) transitions results in double lines for each lower vibrational level. (b) First few lines of the NaK $3^1\Pi$ ($v = 12, J = 30, f$) $\rightarrow 1(X)^1\Sigma^+$ (v', J, e) fluorescence series. The selection rule $\Delta J = 0$ for $^1\Pi$ (f parity) $\rightarrow ^1\Sigma^+$ (e parity) transitions results in single lines for each lower vibrational level.

fluorescence is monitored using a second free-standing PMT (Hamamatsu R928, spectral response 185–900 nm) equipped with a set of three interference filters designed to transmit light in the range 353–462 nm (“PMT – total violet” in Fig. 1).

Removal of a mirror from the fluorescence path on the right-hand side of the heat pipe in Fig. 1 allows resolved $3^1\Pi \rightarrow 1(X)^1\Sigma^+$ fluorescence scans to be obtained with a 0.5-m monochromator equipped with another PMT. These resolved fluorescence scans are taken with both lasers fixed

to the centers of their respective transitions, and signals recorded with the “total violet” PMT are used to correct relative resolved peak intensities for small frequency drifts associated with either laser. Examples of such resolved scans are shown in Figs. 2a and 2b for an e and f parity $3^1\Pi$ level, respectively.

In all cases, the PUMP laser beam was chopped and lock-in detection techniques were employed. A removable mirror in the violet fluorescence path allows light from a calibrated tungsten–halogen white light source to be trans-

TABLE 1

NaK 3¹Π(*v*, *J*, *e/f*) ← 2(A)¹Σ⁺(*v'*, *J'*, *e*) ← 1(X)¹Σ⁺(*v''*, *J''*, *e*) Transitions Identified in This Experiment and Comparison between the Experimentally Measured Energies of the 3¹Π(*v*, *J*, *e/f*) Ro-Vibrational Levels (Referenced to the Bottom of the Ground State Well) and the Energies Obtained from the Molecular State Constants (Table 2) Obtained in This Work

3 ¹ Π (<i>v</i> , <i>J</i> , <i>e/f</i>)	2(A) ¹ Σ ⁺ (<i>v'</i> , <i>J'</i> , <i>e</i>)	1(X) ¹ Σ ⁺ (<i>v''</i> , <i>J''</i> , <i>e</i>)	PUMP frequency (cm ⁻¹)	PROBE frequency (cm ⁻¹)	E[3 ¹ Π (<i>v</i> , <i>J</i> , <i>e/f</i>) (cm ⁻¹) measured value	E[3 ¹ Π (<i>v</i> , <i>J</i> , <i>e/f</i>) (cm ⁻¹) calculated value	E[meas.]-E[calc.] (cm ⁻¹)
4, 9, e	16, 10, e	0, 11, e	13349.1088	12311.9690	25735.4980	25735.4870	0.0110
4, 10, f	16, 10, e	0, 11, e	13349.1088	12313.0810	25736.6100	25736.5988	0.0112
4, 11, e	16, 10, e	0, 11, e	13349.1088	12314.3097	25737.8387	25737.8222	0.0165
5, 9, e	16, 10, e	0, 11, e	13349.1088	12357.1595	25780.6885	25780.6836	0.0049
5, 10, f	16, 10, e	0, 11, e	13349.1088	12358.2588	25781.7878	25781.7821	0.0057
5, 11, e	16, 10, e	0, 11, e	13349.1088	12359.4712	25783.0002	25782.9908	0.0094
6, 9, e	16, 10, e	0, 11, e	13349.1088	12401.7566	25825.2856	25825.2792	0.0064
6, 10, f	16, 10, e	0, 11, e	13349.1088	12402.8419	25826.3709	25826.3638	0.0071
6, 11, e	16, 10, e	0, 11, e	13349.1088	12404.0398	25827.5688	25827.5573	0.0115
7, 9, e	16, 10, e	0, 11, e	13349.1088	12445.6923	25869.2213	25869.2267	-0.0054
7, 10, f	16, 10, e	0, 11, e	13349.1088	12446.7583	25870.2873	25870.2968	-0.0095
7, 11, e	16, 10, e	0, 11, e	13349.1088	12447.9684	25871.4974	25871.4744	0.0230
8, 9, e	16, 10, e	0, 11, e	13349.1088	12488.9479	25912.4769	25912.4787	-0.0018
8, 10, f	16, 10, e	0, 11, e	13349.1088	12490.0062	25913.5352	25913.5338	0.0014
8, 11, e	16, 10, e	0, 11, e	13349.1088	12491.1718	25914.7008	25914.6949	0.0059
9, 9, e	16, 10, e	0, 11, e	13349.1088	12531.4555	25954.9845	25954.9881	-0.0036
9, 10, f	16, 10, e	0, 11, e	13349.1088	12532.4955	25956.0245	25956.0276	-0.0031
9, 11, e	16, 10, e	0, 11, e	13349.1088	12533.6440	25957.1730	25957.1717	0.0013
10, 9, e	16, 10, e	0, 11, e	13349.1088	12573.1742	25996.7032	25996.7076	-0.0044
10, 10, f	16, 10, e	0, 11, e	13349.1088	12574.2090	25997.7380	25997.7311	0.0069
10, 11, e	16, 10, e	0, 11, e	13349.1088	12575.3447	25998.8737	25998.8574	0.0163
11, 10, f	16, 10, e	0, 11, e	13349.1088	12615.1016	26038.6306	26038.5969	0.0337
12, 9, e	16, 10, e	0, 11, e	13349.1088	12654.0344	26077.5634	26077.5883	-0.0249
12, 10, f	16, 10, e	0, 11, e	13349.1088	12655.0290	26078.5580	26078.5779	-0.0199
12, 11, e	16, 10, e	0, 11, e	13349.1088	12656.1256	26079.6546	26079.6670	-0.0124
14, 9, e	16, 10, e	0, 11, e	13349.1088	12731.1754	26154.7044	26154.7430	-0.0386
14, 10, f	16, 10, e	0, 11, e	13349.1088	12732.1348	26155.6638	26155.6965	-0.0327
14, 11, e	16, 10, e	0, 11, e	13349.1088	12733.1952	26156.7242	26156.7460	-0.0218
15, 9, e	16, 10, e	0, 11, e	13349.1088	12768.3143	26191.8433	26191.8050	0.0383
15, 10, f	16, 10, e	0, 11, e	13349.1088	12769.1494	26192.6784	26192.7397	-0.0613
15, 11, e	16, 10, e	0, 11, e	13349.1088	12770.2181	26193.7471	26193.7684	-0.0213
3, 17, e	16, 18, e	0, 17, e	13346.7649	12264.1085	25701.8069	25701.8988	-0.0919
3, 18, f	16, 18, e	0, 17, e	13346.7649	12266.2372	25703.9356	25703.9286	0.0070
3, 19, e	16, 18, e	0, 17, e	13346.7649	12268.3728	25706.0712	25706.0715	-0.0003
4, 17, e	16, 18, e	0, 17, e	13346.7649	12309.8205	25747.5189	25747.5120	0.0069
4, 18, f	16, 18, e	0, 17, e	13346.7649	12311.8198	25749.5182	25749.5191	-0.0009
4, 19, e	16, 18, e	0, 17, e	13346.7649	12313.9349	25751.6333	25751.6382	-0.0049
5, 17, e	16, 18, e	0, 17, e	13346.7649	12354.8777	25792.5761	25792.5654	0.0107
5, 18, f	16, 18, e	0, 17, e	13346.7649	12356.8507	25794.5491	25794.5489	0.0002
5, 19, e	16, 18, e	0, 17, e	13346.7649	12358.9425	25796.6409	25796.6431	-0.0022
6, 17, e	16, 18, e	0, 17, e	13346.7649	12399.3190	25837.0174	25837.0120	0.0054
6, 18, f	16, 18, e	0, 17, e	13346.7649	12401.2666	25838.9650	25838.9708	-0.0058
6, 19, e	16, 18, e	0, 17, e	13346.7649	12403.3202	25841.0186	25841.0391	-0.0205
7, 17, e	16, 18, e	0, 17, e	13346.7649	12443.1087	25880.8071	25880.8043	0.0028
7, 18, f	16, 18, e	0, 17, e	13346.7649	12445.0321	25882.7305	25882.7376	-0.0071
7, 19, e	16, 18, e	0, 17, e	13346.7649	12447.0709	25884.7693	25884.7788	-0.0095
8, 17, e	16, 18, e	0, 17, e	13346.7649	12486.2040	25923.9024	25923.8953	0.0071
8, 18, f	16, 18, e	0, 17, e	13346.7649	12488.0981	25925.7965	25925.8019	-0.0054
8, 19, e	16, 18, e	0, 17, e	13346.7649	12490.1088	25927.8072	25927.8151	-0.0079
9, 17, e	16, 18, e	0, 17, e	13346.7649	12528.5493	25966.2477	25966.2378	0.0099
9, 18, f	16, 18, e	0, 17, e	13346.7649	12530.4195	25968.1179	25968.1167	0.0012
9, 19, e	16, 18, e	0, 17, e	13346.7649	12532.4004	25970.0988	25970.1009	-0.0021
10, 17, e	16, 18, e	0, 17, e	13346.7649	12570.1322	26007.8306	26007.7844	0.0462
10, 18, f	16, 18, e	0, 17, e	13346.7649	12571.9773	26009.6757	26009.6347	0.0410
10, 19, e	16, 18, e	0, 17, e	13346.7649	12573.9229	26011.6213	26011.5887	0.0326
3, 18, e	16, 19, e	0, 18, e	13345.6738	12263.9199	25703.9421	25703.9286	0.0135
3, 19, f	16, 19, e	0, 18, e	13345.6738	12266.0485	25706.0707	25706.0715	-0.0008
3, 20, e	16, 19, e	0, 18, e	13345.6738	12268.2982	25708.3204	25708.3273	-0.0069
4, 18, e	16, 19, e	0, 18, e	13345.6738	12309.5005	25749.5227	25749.5191	0.0036

Note. The uncertainty in each measured level energy is taken to be 0.02 cm⁻¹.

TABLE 1—Continued

$3^1\Pi$ (v, J, e/f)	$2(A)^1\Sigma^+$ (v', J', e)	$1(X)^1\Sigma^+$ (v'', J'', e)	PUMP frequency (cm^{-1})	PROBE frequency (cm^{-1})	$E[3^1\Pi$ (v, J, e/f)] (cm^{-1}) measured value	$E[3^1\Pi$ (v, J, e/f)] (cm^{-1}) calculated value	$E[\text{meas.}] - E[\text{calc.}]$ (cm^{-1})
4, 19, f	16, 19, e	0, 18, e	13345.6738	12311.6104	25751.6326	25751.6382	-0.0056
4, 20, e	16, 19, e	0, 18, e	13345.6738	12313.8343	25753.8565	25753.8689	-0.0124
5, 18, e	16, 19, e	0, 18, e	13345.6738	12354.5311	25794.5533	25794.5489	0.0044
5, 19, f	16, 19, e	0, 18, e	13345.6738	12356.6137	25796.6359	25796.6431	-0.0072
5, 20, e	16, 19, e	0, 18, e	13345.6738	12358.8147	25798.8369	25798.8477	-0.0108
6, 18, e	16, 19, e	0, 18, e	13345.6738	12398.9513	25838.9735	25838.9708	0.0027
6, 19, f	16, 19, e	0, 18, e	13345.6738	12401.0073	25841.0295	25841.0391	-0.0096
6, 20, e	16, 19, e	0, 18, e	13345.6738	12403.1830	25843.2052	25843.2164	-0.0112
7, 18, e	16, 19, e	0, 18, e	13345.6738	12442.7140	25882.7362	25882.7376	-0.0014
7, 19, f	16, 19, e	0, 18, e	13345.6738	12444.7434	25884.7656	25884.7788	-0.0132
7, 20, e	16, 19, e	0, 18, e	13345.6738	12446.8859	25886.9081	25886.9278	-0.0197
8, 18, e	16, 19, e	0, 18, e	13345.6738	12485.7827	25925.8049	25925.8019	0.0030
8, 19, f	16, 19, e	0, 18, e	13345.6738	12487.7837	25927.8059	25927.8151	-0.0092
8, 20, e	16, 19, e	0, 18, e	13345.6738	12489.8965	25929.9187	25929.9347	-0.0160
9, 18, e	16, 19, e	0, 18, e	13345.6738	12528.0995	25968.1217	25968.1167	0.0050
9, 19, f	16, 19, e	0, 18, e	13345.6738	12530.0722	25970.0944	25970.1009	-0.0065
9, 20, e	16, 19, e	0, 18, e	13345.6738	12532.1563	25972.1785	25972.1899	-0.0114
10, 18, e	16, 19, e	0, 18, e	13345.6738	12569.6598	26009.6820	26009.6347	0.0473
10, 19, f	16, 19, e	0, 18, e	13345.6738	12571.5976	26011.6198	26011.5887	0.0311
10, 20, e	16, 19, e	0, 18, e	13345.6738	12573.7503	26013.7725	26013.6461	0.1264
12, 18, e	16, 19, e	0, 18, e	13345.6738	12650.0823	26090.1045	26090.0915	0.0130
12, 19, f	16, 19, e	0, 18, e	13345.6738	12651.9633	26091.9855	26091.9820	0.0035
12, 20, e	16, 19, e	0, 18, e	13345.6738	12653.9508	26093.9730	26093.9728	0.0002
14, 18, e	16, 19, e	0, 18, e	13345.6738	12726.7886	26166.8108	26166.7943	0.0165
14, 19, f	16, 19, e	0, 18, e	13345.6738	12728.6043	26168.6265	26168.6173	0.0092
14, 20, e	16, 19, e	0, 18, e	13345.6738	12730.5246	26170.5468	26170.5370	0.0098
15, 18, e	16, 19, e	0, 18, e	13345.6738	12763.6080	26203.6302	26203.6200	0.0102
15, 19, f	16, 19, e	0, 18, e	13345.6738	12765.3904	26205.4126	26205.4076	0.0050
15, 20, e	16, 19, e	0, 18, e	13345.6738	12767.2741	26207.2963	26207.2901	0.0062
3, 29, e	16, 30, e	0, 31, e	13317.5770	12260.1176	25733.5974	25733.5502	0.0472
3, 30, f	16, 30, e	0, 31, e	13317.5770	12263.4950	25736.9748	25736.8634	0.1114
4, 29, e	16, 30, e	0, 31, e	13317.5770	12305.2649	25778.7447	25778.8153	-0.0706
4, 30, f	16, 30, e	0, 31, e	13317.5770	12308.5936	25782.0734	25782.0923	-0.0189
4, 31, e	16, 30, e	0, 31, e	13317.5770	12312.0563	25785.5361	25785.4581	0.0780
5, 29, e	16, 30, e	0, 31, e	13317.5770	12349.9868	25823.4666	25823.5051	-0.0385
5, 30, f	16, 30, e	0, 31, e	13317.5770	12353.2503	25826.7301	25826.7444	-0.0143
5, 31, e	16, 30, e	0, 31, e	13317.5770	12356.6406	25830.1204	25830.0713	0.0491
6, 29, e	16, 30, e	0, 31, e	13317.5770	12394.0477	25867.5275	25867.5725	-0.0450
6, 30, f	16, 30, e	0, 31, e	13317.5770	12397.2682	25870.7480	25870.7722	-0.0242
6, 31, e	16, 30, e	0, 31, e	13317.5770	12400.6214	25874.1012	25874.0585	0.0427
7, 29, e	16, 30, e	0, 31, e	13317.5770	12437.4289	25910.9087	25910.9701	-0.0614
7, 30, f	16, 30, e	0, 31, e	13317.5770	12440.6144	25914.0942	25914.1287	-0.0345
7, 31, e	16, 30, e	0, 31, e	13317.5770	12443.9012	25917.3810	25917.3727	0.0083
8, 29, e	16, 30, e	0, 31, e	13317.5770	12480.1146	25953.5944	25953.6508	-0.0564
8, 30, f	16, 30, e	0, 31, e	13317.5770	12483.2496	25956.7294	25956.7666	-0.0372
8, 31, e	16, 30, e	0, 31, e	13317.5770	12486.5101	25959.9899	25959.9666	0.0233
9, 29, e	16, 30, e	0, 31, e	13317.5770	12522.0334	25995.5132	25995.5674	-0.0542
9, 30, f	16, 30, e	0, 31, e	13317.5770	12525.1214	25998.6012	25998.6387	-0.0375
9, 31, e	16, 30, e	0, 31, e	13317.5770	12528.3237	26001.8035	26001.7929	0.0106
10, 29, e	16, 30, e	0, 31, e	13317.5770	12563.1549	26036.6347	26036.6725	-0.0378
10, 30, f	16, 30, e	0, 31, e	13317.5770	12566.2023	26039.6821	26039.6978	-0.0157
10, 31, e	16, 30, e	0, 31, e	13317.5770	12569.3974	26042.8772	26042.8045	0.0727
11, 30, f	16, 30, e	0, 31, e	13317.5770	12606.3892	26079.8690	26079.8966	-0.0276
11, 31, e	16, 30, e	0, 31, e	13317.5770	12609.5031	26082.9829	26082.9542	0.0287
12, 29, e	16, 30, e	0, 31, e	13317.5770	12642.7376	26116.2174	26116.2599	-0.0425
12, 30, f	16, 30, e	0, 31, e	13317.5770	12645.6761	26119.1559	26119.1880	-0.0321
12, 31, e	16, 30, e	0, 31, e	13317.5770	12648.7406	26122.2204	26122.1946	0.0258
13, 29, e	16, 30, e	0, 31, e	13317.5770	12681.1249	26154.6047	26154.6476	-0.0429
13, 30, f	16, 30, e	0, 31, e	13317.5770	12684.0316	26157.5114	26157.5246	-0.0132
13, 31, e	16, 30, e	0, 31, e	13317.5770	12687.0473	26160.5271	26160.4787	0.0484
14, 29, e	16, 30, e	0, 31, e	13317.5770	12718.5394	26192.0192	26192.0351	-0.0159
14, 30, f	16, 30, e	0, 31, e	13317.5770	12721.3812	26194.8610	26194.8594	0.0016
14, 31, e	16, 30, e	0, 31, e	13317.5770	12724.3361	26197.8159	26197.7591	0.0568

TABLE 1—Continued

3 ¹ Π (v, J, e/f)	2(A) ¹ Σ ⁺ (v', J', e)	1(X) ¹ Σ ⁺ (v'', J'', e)	PUMP frequency (cm ⁻¹)	PROBE frequency (cm ⁻¹)	E[3 ¹ Π (v, J, e/f)] (cm ⁻¹) measured value	E[3 ¹ Π (v, J, e/f)] (cm ⁻¹) calculated value	E[meas.]-E[calc.] (cm ⁻¹)
15, 29, e	16, 30, e	0, 31, e	13317.5770	12754.8790	26228.3588	26228.3751	-0.0163
15, 30, f	16, 30, e	0, 31, e	13317.5770	12757.6655	26231.1453	26231.1450	0.0003
15, 31, e	16, 30, e	0, 31, e	13317.5770	12760.5643	26234.0441	26233.9887	0.0554
3, 55, e	16, 56, e	0, 57, e	13236.4530	12222.5443	25832.4833	25832.5306	-0.0473
3, 56, f	16, 56, e	0, 57, e	13236.4530	12227.2200	25837.1590	25837.0974	0.0616
3, 57, e	16, 56, e	0, 57, e	13236.4530	12232.0388	25841.9778	25842.0436	-0.0658
4, 55, e	16, 56, e	0, 57, e	13236.4530	12266.5997	25876.5387	25876.5730	-0.0343
4, 56, f	16, 56, e	0, 57, e	13236.4530	12271.2179	25881.1569	25881.0838	0.0731
4, 57, e	16, 56, e	0, 57, e	13236.4530	12275.9788	25885.9178	25885.9736	-0.0558
5, 55, e	16, 56, e	0, 57, e	13236.4530	12310.0171	25919.9561	25919.9790	-0.0229
5, 56, f	16, 56, e	0, 57, e	13236.4530	12314.5816	25924.5206	25924.4308	0.0898
5, 57, e	16, 56, e	0, 57, e	13236.4530	12319.2831	25929.2221	25929.2610	-0.0389
6, 55, e	16, 56, e	0, 57, e	13236.4530	12352.8096	25962.7486	25962.7016	0.0470
6, 56, f	16, 56, e	0, 57, e	13236.4530	12357.1609	25967.0999	25967.0912	0.0087
6, 57, e	16, 56, e	0, 57, e	13236.4530	12361.8995	25971.8385	25971.8587	-0.0202
7, 55, e	16, 56, e	0, 57, e	13236.4530	12394.7618	26004.7008	26004.6935	0.0073
7, 56, f	16, 56, e	0, 57, e	13236.4530	12399.1129	26009.0519	26009.0178	0.0341
7, 57, e	16, 56, e	0, 57, e	13236.4530	12403.7598	26013.6988	26013.7195	-0.0207
8, 55, e	16, 56, e	0, 57, e	13236.4530	12435.9484	26045.8874	26045.9074	-0.0200
8, 56, f	16, 56, e	0, 57, e	13236.4530	12440.3191	26050.2581	26050.1633	0.0948
8, 57, e	16, 56, e	0, 57, e	13236.4530	12444.8305	26054.7695	26054.7961	-0.0266
9, 55, e	16, 56, e	0, 57, e	13236.4530	12476.3328	26086.2718	26086.2962	-0.0244
9, 56, f	16, 56, e	0, 57, e	13236.4530	12480.6320	26090.5710	26090.4807	0.0903
9, 57, e	16, 56, e	0, 57, e	13236.4530	12485.1029	26095.0419	26095.0413	0.0006
10, 55, e	16, 56, e	0, 57, e	13236.4530	12515.8409	26125.7799	26125.8126	-0.0327
10, 56, f	16, 56, e	0, 57, e	13236.4530	12520.0755	26130.0145	26129.9226	0.0919
11, 55, e	16, 56, e	0, 57, e	13236.4530	12554.4012	26164.3402	26164.4094	-0.0692
11, 56, f	16, 56, e	0, 57, e	13236.4530	12558.5605	26168.4995	26168.4418	0.0577
11, 57, e	16, 56, e	0, 57, e	13236.4530	12562.8650	26172.8040	26172.8487	-0.0447
12, 55, e	16, 56, e	0, 57, e	13236.4530	12591.9807	26201.9197	26202.0394	-0.1197
12, 56, f	16, 56, e	0, 57, e	13236.4530	12596.0670	26206.0060	26205.9910	0.0150
12, 57, e	16, 56, e	0, 57, e	13236.4530	12600.2844	26210.2234	26210.3164	-0.0930
14, 56, f	16, 56, e	0, 57, e	13236.4530	12667.9773	26277.9163	26277.9910	-0.0747
14, 57, e	16, 56, e	0, 57, e	13236.4530	12672.3564	26282.2954	26282.1439	0.1515

mitted through the heat-pipe oven to the monochromator, to calibrate the relative detection system efficiency versus wavelength (18). Since the fluorescence is partially polarized, the polarization dependence of the detection system efficiency must be taken into account (19). The wavemeter of the PUMP laser was calibrated by recording iodine laser-induced fluorescence and comparing line positions to those given in the iodine atlas (20). The wavemeter of the PROBE laser was calibrated with optical galvanic signals from neon transitions in a hollow-cathode lamp. Energies of 3¹Π state ro-vibrational levels, obtained in this manner, are considered accurate to ~0.02 cm⁻¹.

III. ANALYSIS AND RESULTS

When exciting a 1¹Π state from a single ro-vibrational level of a 1¹Σ⁺ state, a set of three lines (*P*, *Q*, and *R* lines)

can be observed for each 1¹Π state vibrational level. In the present context, where the intermediate state is known to be a 1¹Σ⁺ state, this three line pattern unambiguously identifies the upper state as a 1¹Π state. Comparison with theoretical calculations of NaK potential curves (see sec. IV) allows us to further identify this state as the NaK 3¹Π state correlating to the Na(3S_{1/2}) + K(3D_{3/2}) asymptotic limit (see also Fig. 9 of Ref. (4)).

Also, for a 1¹Π state, all rotational energy levels occur as pairs with opposite *ef* (rotationless) parity (Λ doubling). Thus, for a particular intermediate level 2(A)¹Σ⁺(v', J', e), the three observed lines can be assigned as follows: 3¹Π(v, J' - 1, e) ← 2(A)¹Σ⁺(v', J', e) (*P* line), 3¹Π(v, J', f) ← 2(A)¹Σ⁺(v', J', e) (*Q* line), and 3¹Π(v, J' + 1, e) ← 2(A)¹Σ⁺(v', J', e) (*R* line), due to the selection rules $\Delta J = \pm 1$ for *e* ↔ *e* and $\Delta J = 0$ for *f* ↔ *e*. By using several intermediate levels, the energies of a large number of *e* and *f* parity ro-vibrational levels of the 3¹Π state can be determined. In the present work, five intermediate levels 2(A)¹Σ⁺

($v' = 16, J' = 10, e$), $2(A)^1\Sigma^+$ ($v' = 16, J' = 18, e$), $2(A)^1\Sigma^+$ ($v' = 16, J' = 19, e$), $2(A)^1\Sigma^+$ ($v' = 16, J' = 30, e$), and $2(A)^1\Sigma^+$ ($v' = 16, J' = 56, e$) were used to observe 156 levels of the $3^1\Pi$ state with vibrational numbers in the range $v = 3-15$. The absolute $3^1\Pi$ state vibrational numbering can be determined unambiguously from the comparison of experimental and calculated Franck–Condon factors. These 156 levels, including PUMP and PROBE laser frequencies, are listed in Table 1.

The molecular $3^1\Pi$ state energy levels can be fit using a standard Dunham expansion:

$$E(v, J) = \sum_{i,k} (Y_{i,k} + \delta y_{i,k}) (v + \frac{1}{2})^i [J(J+1) - \Lambda^2]^k, \quad [1]$$

where the $y_{i,k}$ constants describe the Λ doubling of the $^1\Pi$ state ($y_{i,k} = 0$ for $k = 0$) and $\delta = 0$ or 1 for the f and e parity levels, respectively (21–23). (Alternatively, one can use the convention $\delta = -1$ for f and $\delta = +1$ for e levels (24–25).) The molecular constants obtained from a fit to our $3^1\Pi$ state data (26) are listed in Table 2. In the present work, experimental uncertainties proved to be too large to allow assignment of Λ -doubling constants. The higher order coefficients that were included in the fit are necessary to improve the agreement between measured and calculated intensities (see

TABLE 2

The Molecular Constants of the NaK $3^1\Pi$ State Obtained in This Work along with the Theoretical Constants of Ref. (32)

	Experiment (this work)	Theory (Ref. 32)
R_e	4.4761 ± 0.018	4.51
D_e	$1290.9 \pm .5$	1155
$Y_{0,0}$	25520.750 ± 0.12	25568
$Y_{1,0}$	47.5424 ± 0.047	47.20
$Y_{2,0}$	-0.1694 ± 0.0052	
$Y_{3,0}$	$-7.87 \text{E-}3 \pm 1.8\text{E-}4$	
$Y_{0,1}$	$0.058195 \pm .00048$	
$Y_{1,1}$	$-5.337\text{E-}4 \pm 1.4\text{E-}5$	
$Y_{2,1}$	$-1.38\text{E-}5 \pm 5.6\text{E-}7$	
$Y_{0,2}$	$2.09\text{E-}7 \pm 1.5\text{E-}6$	
$Y_{1,2}$	$2.30\text{E-}8 \pm 2.6\text{E-}9$	
$Y_{0,3}$	$6.61\text{E-}10 \pm 1.6\text{E-}9$	
$Y_{0,4}$	$-1.356\text{E-}12 \pm 6.3\text{E-}13$	
$Y_{0,5}$	$2.70\text{E-}16 \pm 8.0\text{E-}17$	

Note. All values are given in cm^{-1} except for the equilibrium internuclear separation R_e which is in \AA . The dissociation energy D_e was obtained from the expression $D_e = [D_e(X^1\Sigma^+) + \Delta E_{\text{atomic}} - Y_{0,0}]$ with $D_e(X^1\Sigma^+) = (5274.9 \pm 0.5) \text{cm}^{-1}$ from Ref. (30) and $\Delta E_{\text{atomic}} = E[\text{Na}(3S_{1/2}) + \text{K}(3D_{3/2})] - E[\text{Na}(3S_{1/2}) + \text{K}(4S_{1/2})] = 21\,536.75 \text{cm}^{-1}$ from Ref. (34). Quoted uncertainties represent 95% confidence limits.

TABLE 3
RKR Turning Points for the NaK $3^1\Pi$ State Obtained in This Work

v	$R_1(\text{\AA})$	$R_2(\text{\AA})$	$E(\text{cm}^{-1})$
-1/2	4.4761	4.4761	0.0000
0	4.2667	4.7103	23.7279
1	4.1284	4.8993	70.9059
2	4.0405	5.0396	117.6743
3	3.9736	5.1606	163.9858
4	3.9190	5.2711	209.7933
5	3.8728	5.3751	255.0495
6	3.8328	5.4748	299.7072
7	3.7976	5.5719	343.7191
8	3.7663	5.6673	387.0381
9	3.7383	5.7618	429.6169
10	3.7131	5.8562	471.4083
11	3.6902	5.9509	512.3652
12	3.6694	6.0464	552.4402
13	3.6505	6.1432	591.5861
14	3.6331	6.2418	629.7558
15	3.6172	6.3425	666.9020
16	3.6026	6.4458	702.9774
17	3.5891	6.5522	737.9350
18	3.5767	6.6622	771.7274
19	3.5652	6.7763	804.3074
20	3.5545	6.8951	835.6278
21	3.5444	7.0194	865.6414
22	3.5349	7.1499	894.3010

below). A comparison between the experimental energy levels and those calculated from the fitted molecular constants is given in Table 1.

The experimental molecular constants can be used to construct an RKR potential curve using standard computer programs (27–28). RKR turning points obtained in this manner for the NaK $3^1\Pi$ state are listed in Table 3 and are plotted in Fig. 3.

Finally, the $3^1\Pi$ state RKR curve can be used to calculate Franck–Condon factors for various $3^1\Pi(v, J, f) \rightarrow 1(X)^1\Sigma^+(v'', J, e)$ and $3^1\Pi(v, J, e) \rightarrow 1(X)^1\Sigma^+(v'', J \pm 1, e)$ transitions (27, 29). For these calculations, the ground state constants of Ref. (30) were used. In the present case, the entire $3^1\Pi(v, J) \rightarrow 1(X)^1\Sigma^+$ band can be observed, and because the difference potential is monotonic over the range of internuclear separations (R values) accessed by this experiment, a counting of the nodes of the Franck–Condon envelope function yields an unambiguous determination of the absolute $3^1\Pi$ state vibrational numbering. This is confirmed by comparisons between experimental and calculated Franck–Condon factors obtained with different upper state vibrational numbering assignments.

The relative intensities of peaks in the $3^1\Pi \rightarrow 1^1\Sigma^+$ resolved fluorescence scans are given by the following formula (17, 25):

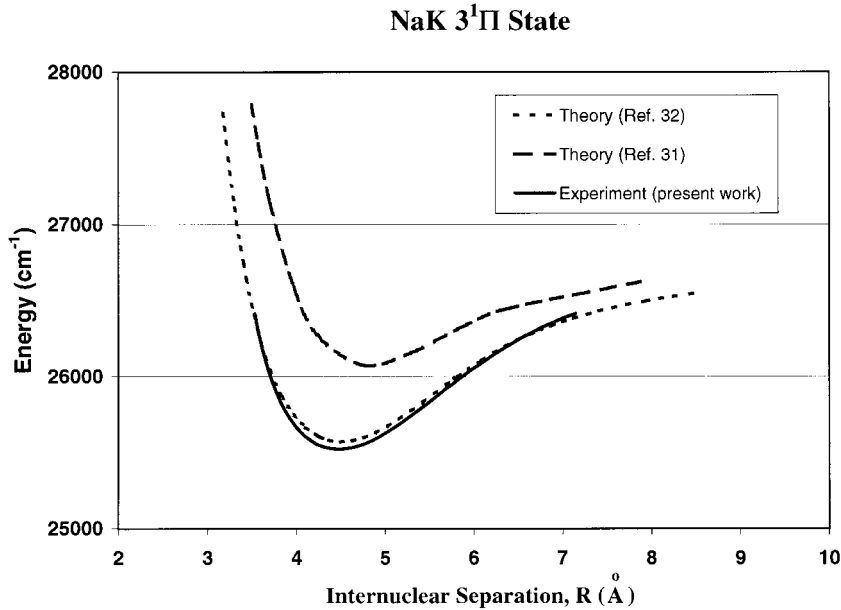


FIG. 3. Comparison of the experimental NaK 3¹Π state RKR potential curve (solid line) obtained in the present work, with the theoretical 3¹Π state potentials of Ref. (32) (dotted line) and Ref. (31) (dashed line).

$$I_{\tilde{n}}(v, J \rightarrow v', J')$$

$$= \frac{64\pi^4}{3} N_{v,J} \frac{S_{J,J'}}{2J+1} \frac{v^4}{c^3} \left| \int \psi_{v,J} M_e(R) \psi_{v',J'} dR \right|^2. \quad [2]$$

Here $N_{v,J}$ is the number of molecules in the upper level, $S_{J,J'}$ is the Hönl–London factor (17), and $M_e(R) = \langle \psi_{3^1\Pi}(R) | \sum_i e\mathbf{r}_i | \psi_{1^1\Sigma^+}(R) \rangle$ is the electronic transition dipole moment with respect to the Born–Oppenheimer wavefunctions $\psi_{3^1\Pi}(R)$ and $\psi_{1^1\Sigma^+}(R)$ (which depend parametrically on R). If it is assumed that the electronic transition dipole moment does not vary appreciably with R , then the dipole moment can be removed from the integral and this expression reduces to

$$I_{\tilde{n}}(v, J \rightarrow v', J')$$

$$= \frac{64\pi^4}{3} N_{v,J} \frac{S_{J,J'}}{2J+1} \frac{v^4}{c^3} [M_e(R)]^2 \left| \int \psi_{v,J} \psi_{v',J'} dR \right|^2, \quad [3]$$

where $|\int \psi_{v,J} \psi_{v',J'} dR|^2$ is the Franck–Condon factor. Thus we can compare experimental 3¹Π → 1¹Σ⁺ relative intensities with calculated Franck–Condon factors multiplied by v^4 . To improve the quality of the comparison, the experimental relative intensities are also corrected for the relative detection system efficiency (obtained as described in sec. II using the calibrated tungsten–halogen white lamp). They are also divided by the total violet band fluorescence

intensity, which is continuously monitored during the resolved fluorescence scans, to correct for small laser frequency drifts.

Figure 4 shows this comparison for a few selected 3¹Π ro-vibrational levels. In each case, the calculated intensities are normalized to the experimental intensities at the maximum experimental intensity peak. Here it can be seen that the node positions are reproduced with reasonable accuracy. However, it is apparent that the calculations do not predict the observed reduction of intensity with increasing wavelength. This failure is due to the assumption that the dipole moment is constant with internuclear separation. In fact, the transition dipole moment is expected to decrease with increasing internuclear separation since the molecular emission (at small R) is fully allowed, while the asymptotic atomic transition, Na(3S) + K(3D) → Na(3S) + K(4S) (at $R \rightarrow \infty$), is dipole forbidden. We attempted to fit the calculated intensities to the experimental intensities with Eq. [2] using a dipole moment that varies linearly with R ; i.e.,

$$M_e(R) = m_0 + m_1(R - R_{eq}), \quad [4]$$

where $R_{eq} = 4.4761 \text{ \AA}$ is the equilibrium separation of the 3¹Π state. Although this produced much better agreement than the Condon approximation, $M_e(R) = \text{constant}$, it became clear that a more complicated function was needed. Using the computer program LEVEL 6.0 (29), it

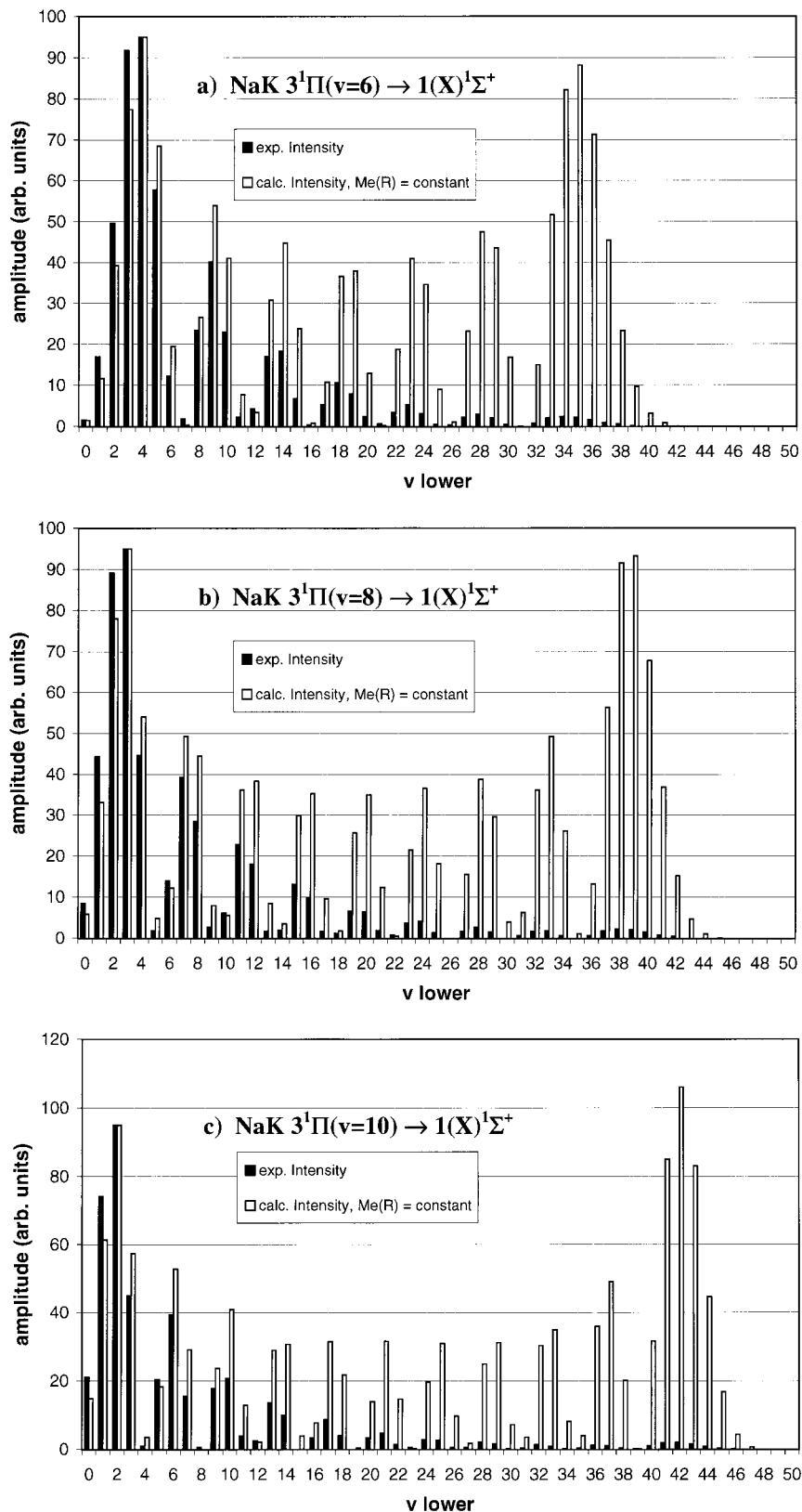


FIG. 4. Experimental and calculated relative intensities for transitions from $3^1\Pi(v, J = 30, f)$ to different $1(X)^1\Sigma^+(v', J = 30, e)$ levels. (a) $v = 6$, (b) $v = 8$, (c) $v = 10$, (d) $v = 12$. In these calculations, the transition dipole moment was taken to be constant with internuclear separation. Experimental and calculated values are normalized to each other at the highest intensity experimental peak.

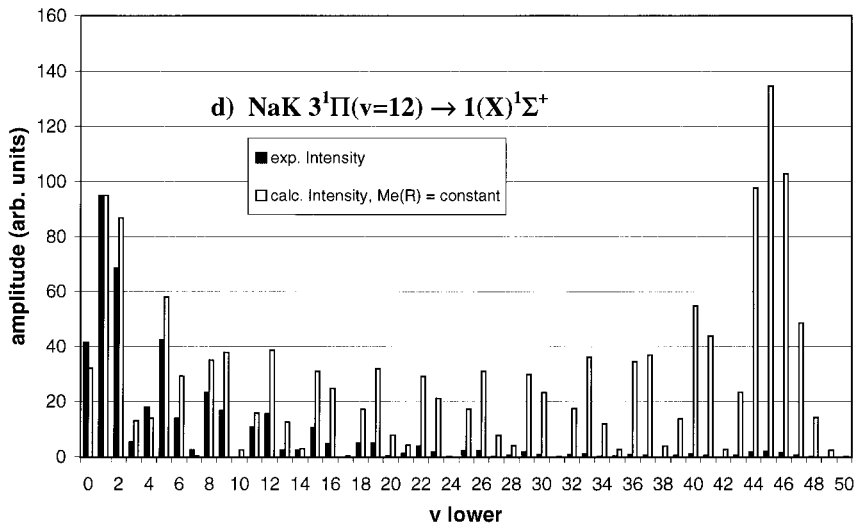


FIG. 4—Continued

is straightforward to expand the dipole moment function in either powers of R or powers of R^{-2} . In the end, we found that good agreement between the calculated and experimental intensities could be obtained by using a function of the form

$$M_e(R) = p_1 R^{-2} + p_2 R^{-4} + p_3 R^{-6} + p_4 R^{-8} + p_5 R^{-10}, \quad [5]$$

with $p_2/p_1 = -76.3 (\text{\AA})^2$, $p_3/p_1 = 2157 (\text{\AA})^4$, $p_4/p_1 = -24\,300 (\text{\AA})^6$, and $p_5/p_1 = 97\,850 (\text{\AA})^8$, or alternatively

$$M_e(R) = m_0 + m_1(R - R_{eq}) + m_2(R - R_{eq})^2 + m_3(R - R_{eq})^3 + m_4(R - R_{eq})^4, \quad [6]$$

with $m_1/m_0 = -1.2677 (\text{\AA})^{-1}$, $m_2/m_0 = 0.6795 (\text{\AA})^{-2}$, $m_3/m_0 = -0.07907 (\text{\AA})^{-3}$, and $m_4/m_0 = -0.01267 (\text{\AA})^{-4}$. These parameters were determined by trial and error while attempting to minimize the weighted mean-squared residuals. Figure 5 shows a comparison of the experimental intensities with those calculated using Eq. [5] in Eq. [2]. These results should be contrasted with those shown in Fig. 4, where $M_e(R) = \text{constant}$ was assumed. Again, only relative intensities can be compared, so the experimental and theoretical intensities have been normalized in each case at the highest intensity peak. The relative transition dipole moment determined in this manner is plotted in Fig. 6 and should be considered to be valid for internuclear separations in the range $R = 3.4\text{--}6.6 \text{\AA}$. It should be noted that the functional forms for $M_e(R)$ given in Eqs. [5] and [6] are not physical and simply provide convenient analytic expressions to represent the transition dipole moment over the range of R values accessed by this experiment. From a physical stand-

point, Eq. [5] for the dipole moment may be preferable since it goes to zero at large internuclear separation as the true dipole moment function must. However, we warn against extrapolation using either expression beyond the range plotted in Fig. 6 since our experiment provides no information beyond this range.

IV. DISCUSSION

Stevens *et al.* (31) have calculated all NaK potentials up to the Na(3S) + K(3D) dissociation limit and Δ states corresponding to the Na(3S) + K(4S) and Na(4P) + K(4P) limits using full-valence configuration interaction computations with effective core potentials. More recently, Magnier and Milli  (32) used pseudopotential methods to calculate potentials up to the Na(3P) + K(4P) limit. The theoretical 3¹Π potential curves from these two studies are compared to the present experimental potential in Fig. 3. The theoretical molecular constants of Ref. (32) are also listed in Table 2 in comparison to the present experimental values. It can be seen that very good agreement exists between the present experimental results and recent theoretical calculations for this NaK 3¹Π state. Earlier we found good agreement between our experimental results for the NaK 6¹Σ⁺ state (4) and the calculations of Magnier and Milli  (32). Thus it appears that the theoretical NaK potentials of Magnier and Milli  are of very high quality, even for relatively high-lying electronic states. High-quality experimental and theoretical potential curves in this energy range will likely be important for future NaK cold atom photoassociation experiments.

The present results can also be used to test theoretical dipole moment functions for the NaK 3¹Π → 1(X)¹Σ⁺ band as they

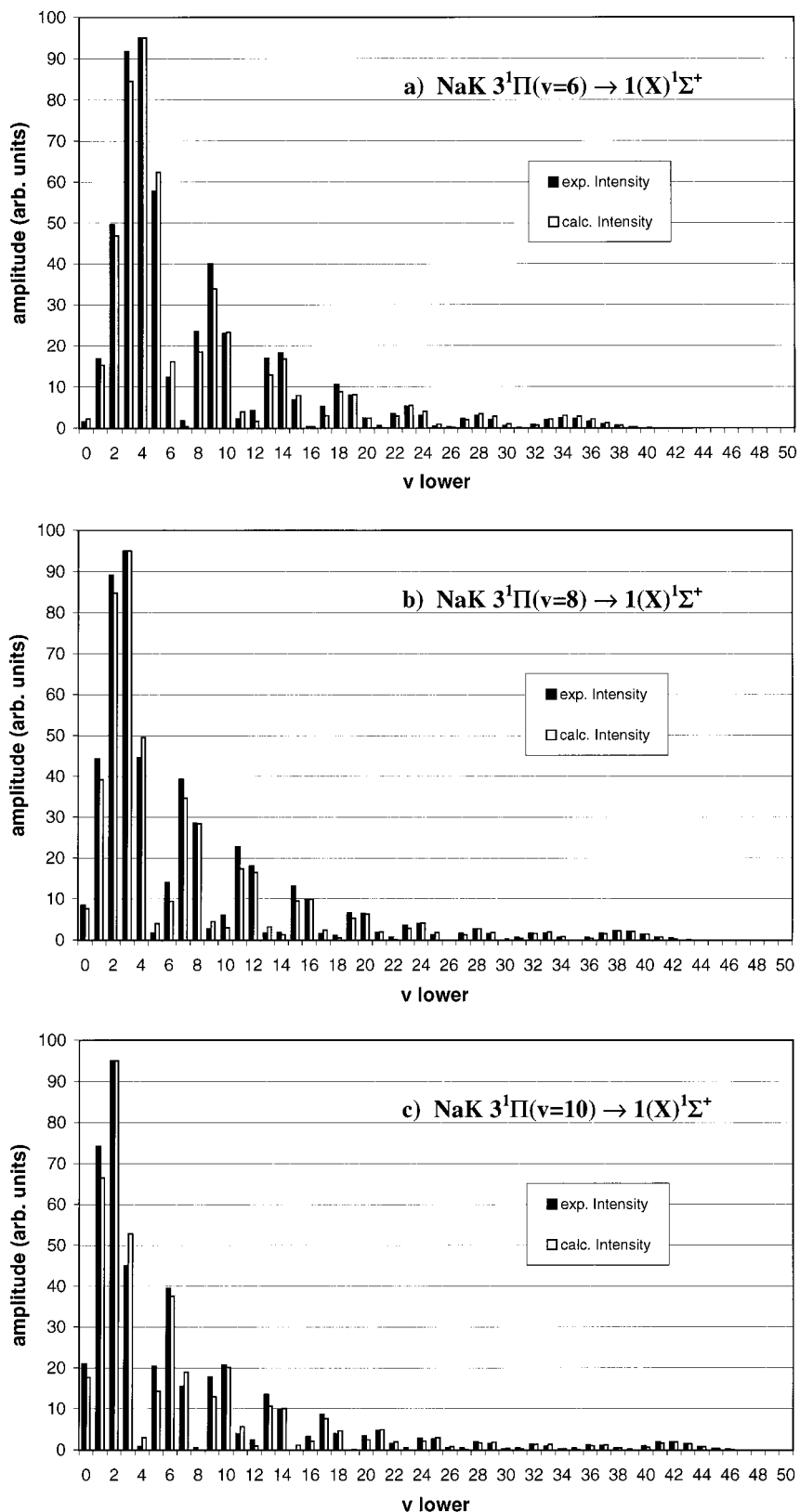


FIG. 5. Experimental and calculated relative intensities for transitions from $3^1\Pi$ ($v, J = 30, f$) to different $1(X)^1\Sigma^+$ ($v', J = 30, e$) levels. (a) $v = 6$, (b) $v = 8$, (c) $v = 10$, (d) $v = 12$. In these calculations, the transition dipole moment was taken to be $M_e(R) = p_1 R^{-2} + p_2 R^{-4} + p_3 R^{-6} + p_4 R^{-8} + p_5 R^{-10}$ with $p_2/p_1 = -76.3$ (\AA^2), $p_3/p_1 = 2157$ (\AA^4), $p_4/p_1 = -24\,300$ (\AA^6), and $p_5/p_1 = 97\,850$ (\AA^8). Experimental and calculated values are normalized to each other at the highest intensity peak.

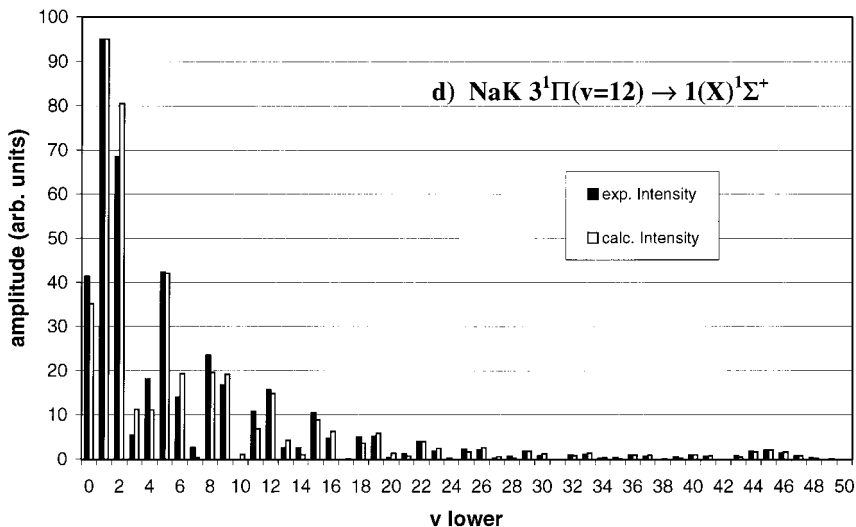


FIG. 5—Continued

become available. Figure 6 compares the experimental dipole moment determined in the present work with one early calculation (33). Although the calculation reproduces the basic trend that the dipole moment decreases with R , it is clear that the calculated slope is much too small. We hope that the current measurements will motivate new calculations of this dipole moment in the near future.

NaK $3^1\Pi \rightarrow 1(X)^1\Sigma^+$ Transition Dipole Moment

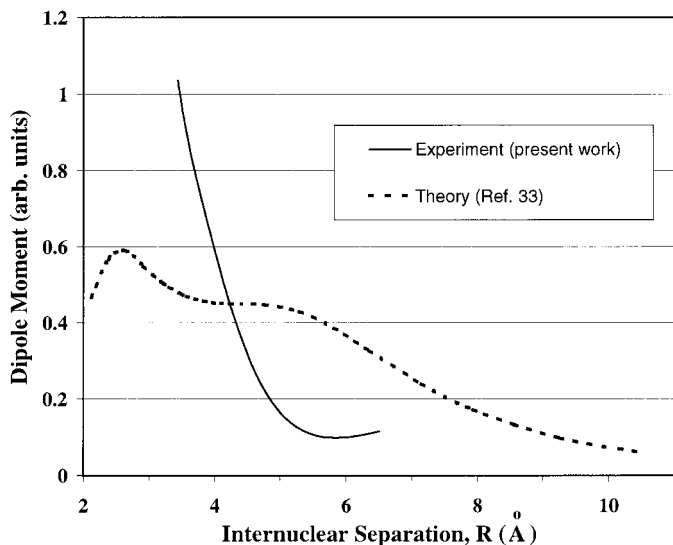


FIG. 6. Solid line: experimental NaK $3^1\Pi \rightarrow 1(X)^1\Sigma^+$ relative transition dipole moment versus internuclear separation obtained in this work [$M_e(R) = p_1 R^{-2} + p_2 R^{-4} + p_3 R^{-6} + p_4 R^{-8} + p_5 R^{-10}$ with $p_2/p_1 = -76.3 (\text{\AA})^2$, $p_3/p_1 = 2157 (\text{\AA})^4$, $p_4/p_1 = -24\,300 (\text{\AA})^6$, and $p_5/p_1 = 97\,850 (\text{\AA})^8$]. Dotted line: theoretical transition dipole moment from Ref. (33). The two curves are normalized to each other at $R = 4.23 \text{ \AA}$ (8.0 a.u.).

ACKNOWLEDGMENTS

The authors thank Prof. A. M. Lyyra, Prof. Li Li, and Guenadiy Lazarov for many valuable discussions on this work and for providing copies of RKR and Franck–Condon factor computer programs. We also thank Prof. R. J. LeRoy for helpful discussions on fitting the transition dipole moment function and for making computer programs DSParFit, RKR1, and LEVEL 6.0 available to us. Finally, we acknowledge financial support for this work from the National Science Foundation under Grants PHY-9119498 and PHY-9322015. Ian Mazsa, Suzanne Webb, and Jeanette La Civita were all supported through the NSF Research Experiences for Undergraduates (REU) program.

Note added in proof. After submission of the present manuscript, an experimental study of the NaK $3^1\Pi$ and $6^1\Sigma^+$ states was published by Pashov *et al.* [*Phys. Rev. A* **58**, 1048 (1998)]. These authors carried out a comprehensive mapping of both states using polarization labeling spectroscopy. Pashov *et al.* point out that the $6^1\Sigma^+$ state vibrational numbering reported in our earlier work (4) was incorrect by one unit due to the limited data set and long extrapolation (more than 1100 cm^{-1}) to the bottom of the potential well. Therefore the Pashov results for the $6^1\Sigma^+$ state molecular constants and RKR potential should be considered superior to those reported in Ref. (4). (The principal results of Ref. (4), which are the absolute predissociation rates for individual rovibrational levels, remain valid except that all vibrational assignments in Ref. (4) should be increased by one unit.) The present results for the $3^1\Pi$ state molecular constants are in fairly good agreement with those of Pashov *et al.* for $J \leq 31$. However, the Pashov results for the $3^1\Pi$ state constants and potential curve are also probably more accurate than those of the present study since the former are based on a larger data field and use of the more accurate inverted perturbation approach (IPA) method. Pashov *et al.* did not study the $3^1\Pi \rightarrow 1(X)^1\Sigma^+$ electronic transition dipole moment reported here.

REFERENCES

1. A. Yiannopoulou, K. Urbanski, S. Antonova, A. M. Lyyra, L. Li, T. An, T. J. Whang, B. Ji, X. T. Wang, W. C. Stwalley, T. Leininger, and G.-H. Jeung, *J. Chem. Phys.* **103**, 5898 (1995).
2. B. Ji, C.-C. Tsai, L. Li, T.-J. Whang, A. M. Lyyra, H. Wang, J. T. Bahns, W. C. Stwalley, and R. J. LeRoy, *J. Chem. Phys.* **103**, 7240 (1995).

3. L. Li, A. Yiannopoulou, K. Urbanski, A. M. Lyra, B. Ji, W. C. Stwalley, and T. An, *J. Chem. Phys.* **105**, 6192 (1995).
4. Z. J. Jabbour and J. Huennekens, *J. Chem. Phys.* **107**, 1094 (1997).
5. R. A. Bernheim, L. P. Gold, and T. Tipton, *J. Chem. Phys.* **78**, 3635 (1983).
6. S. B. Rai, B. Hemmerling, and W. Demtröder, *Chem. Phys.* **97**, 127 (1985).
7. D. A. Miller, L. P. Gold, P. D. Tripodi, and R. A. Bernheim, *J. Chem. Phys.* **92**, 5822 (1990).
8. C. Linton, F. Martin, P. Crozet, A. J. Ross, and R. Bacis, *J. Mol. Spectrosc.* **158**, 445 (1993).
9. J. T. Kim, H. Wang, J. T. Bahns, and W. C. Stwalley, *J. Chem. Phys.* **102**, 6966 (1995).
10. M. Schwarz, R. Duchowicz, W. Demtröder, and Ch. Jungen, *J. Chem. Phys.* **89**, 5460 (1988).
11. C.-C. Tsai, J. T. Bahns, and W. C. Stwalley, *J. Chem. Phys.* **100**, 768 (1994).
12. C.-C. Tsai, J. T. Bahns, and W. C. Stwalley, *J. Mol. Spectrosc.* **167**, 429 (1994).
13. C.-C. Tsai, J. T. Bahns, H. Wang, T.-J. Whang, and W. C. Stwalley, *J. Chem. Phys.* **101**, 25 (1994).
14. A. J. Taylor, K. M. Jones, and A. L. Schawlow, *J. Opt. Soc. Am.* **73**, 994 (1983).
15. S. Kasahara, H. Ikoma, and H. Katô, *J. Chem. Phys.* **100**, 63 (1994).
16. L. Li and R. W. Field, *J. Phys. Chem.* **87**, 3020 (1983).
17. G. Herzberg, "Molecular Spectra and Molecular Structure I. Spectra of Diatomic Molecules," Krieger, Malabar, 1989.
18. R. Stair, W. E. Schneider, and J. K. Jackson, *Appl. Opt.* **2**, 1151 (1963).
19. H. Chen, L. Li, G. Lazarov, A. M. Lyra, J. Huennekens, and R. W. Field, unpublished manuscript.
20. S. Gerstenkorn and P. Luc, "Atlas du Spectre D'Absorption de la Molécule D'Iode," Centre National de la Recherche Scientifique, Paris, 1978.
21. R. S. Mulliken and A. Christy, *Phys. Rev.* **38**, 87 (1931).
22. J. M. Brown and A. J. Merer, *J. Mol. Spectrosc.* **74**, 488 (1979).
23. I. Jackowska, W. Jastrzebski, and P. Kowalczyk, *J. Phys. B* **29**, L561 (1996).
24. G. Herzberg, "Molecular Spectra and Molecular Structure III. Electronic Structure of Polyatomic Molecules," Krieger, Malabar, 1991.
25. P. F. Bernath, "Spectra of Atoms and Molecules," Oxford Univ. Press, New York, 1995.
26. R. J. LeRoy, "DSParFit: Least-Squares Data Fitting Program," University of Waterloo, Department of Chemistry, unpublished; "Improved Parameterization for Diatom Born-Oppenheimer Breakdown Effects, and a New Combined-Isotopes Analysis for HF and DF," University of Waterloo, Chemical Physics Research Report No. CP-633.
27. K. M. Sando, computer programs "RKR," "Spline," "Eigen," "FCF," University of Iowa, Department of Chemistry, unpublished.
28. R. J. LeRoy, "RKR1: A Computer Program Implementing the First-Order RKR Method for Determining Diatom Potential Energy Curves from Spectroscopic Constants," University of Waterloo, Chemical Physics Research Report No. CP-425, 1992.
29. R. J. LeRoy, "LEVEL 6.0: A Computer Program Solving the Radial Schrodinger Equation for Bound and Quasibound Levels, and Calculating Various Expectation Values and Matrix Elements," University of Waterloo, Chemical Physics Research Report No. CP-555, 1995.
30. A. J. Ross, C. Effantin, J. d'Incan, and R. F. Barrow, *Mol. Phys.* **56**, 903 (1985).
31. W. J. Stevens, D. D. Konowalow, and L. B. Ratcliff, *J. Chem. Phys.* **80**, 1215 (1984).
32. S. Magnier and Ph. Millié, *Phys. Rev. A* **54**, 204 (1996).
33. L. B. Ratcliff, D. D. Konowalow, and W. J. Stevens, *J. Mol. Spectrosc.* **110**, 242 (1985).
34. C. E. Moore, "Atomic Energy Levels," National Bureau of Standards Circular 467, Vol. 1, U.S. Government Printing Office, Washington, DC, 1949.